References and Notes

1. H. S. Bridge, A. J. Lazarus, J. D. Scudder, K. W. Ogilvie, R. E. Hartle, J. R. Asbridge, S. J. Bame, W. C. Feldman, G. L. Siscoe, *Science* **183**, 1293 (1974).
2. M. D. Montgomery, J. R. Asbridge, S. J. Bame, *J. Geophys. Res.* **75**, 1217 (1970); J. D. Scudder, D. L. Lind, K. W. Ogilvie, *ibid.* **78**, 6535 (1973); W. C. Feldman, M. D. Montgomery, J. R. Asbridge, S. J. Bame, H. R. Lewis, paper presented at the 3rd Solar Wind Conference (Asilomar, Calif., 1974).
3. N. F. Ness, K. W. Behannon, R. P. Lepping, Y. C. Whang, K. H. Schatten, *Science* **185**, 151 (1974).
4. K. W. Ogilvie, J. D. Scudder, M. Sugiura, *J. Geophys. Res.* **76**, 3574 (1971); S. J. Bame, J. R. Asbridge, H. E. Felthauser, E. W. Hones, I. B. Strong, *ibid.* **72**, 113 (1967).
5. E. W. Greenstadt, I. M. Green, G. T. Inouye, D. S. Colburn, J. H. Binsack, E. F. Lyon, *Cosmic Electrodyn.* **1**, 160 (1970); E. W. Greenstadt, *J. Geophys. Res.* **77**, 1729 (1972); D. H. Fairfield, *ibid.* **74**, 3541 (1969).
6. K. A. Anderson, *J. Geophys. Res.* **74**, 95 (1969); F. L. Scarf, F. L. Fredricks, L. A. Frank, M. Neugebauer, *ibid.* **78**, 3697 (1973); W. C. Feldman, J. R. Asbridge, S. J. Bame, M. D. Montgomery, *ibid.* p. 3697.
7. J. A. Simpson, J. H. Eraker, J. E. Lamport, P. H. Walpole, *Science* **185**, 160 (1974).
8. A. L. Broadfoot *et al.*, *ibid.*, p. 166.
9. L. Bierman, B. Brosowski, H. Schmidt, *Solar Phys.* **1**, 254 (1967); P. A. Cloutier, M. B. McElroy, F. C. Michael, *J. Geophys. Res.* **74**, 6215 (1969); R. E. Hartle, S. J. Bauer, C. S. Wu, *Int. Assoc. Geophys. Aeron. Bull.* **34**, 569 (1973).
10. G. L. Siscoe and N. R. Mukherjee, *J. Geophys. Res.* **78**, 3961 (1973).
11. H. T. Howard *et al.*, *Science* **185**, 179 (1974).
12. J. R. Spreiter, A. L. Summers, A. W. Rizzi, *Planet. Space Sci.* **18**, 1281 (1970).
13. C. P. Sonett and D. S. Colburn, *Nature (Lond.)* **216**, 340 (1967); A. J. Dessler, in *Atmospheres of Venus and Mars*, J. C. Brandt and M. B. McElroy, Eds. (Gordon & Breach, London, 1968), pp. 241–250; F. S. Johnson and J. E. Midgley, *J. Geophys. Res.* **73**, 1523 (1968); J. V. Holweg, *ibid.*, p. 7269; G. Schubert *et al.*, *NASA Tech. Mem. X-62* (1973), p. 227.
14. G. L. Siscoe, K. W. Behannon, R. P. Lepping, N. F. Ness, *Geophys. Res. Lett.*, in press.
15. S. E. deForest, *J. Geophys. Res.* **77**, 651 (1972).

16. We thank all those whose work contributed to the success of the experiment and those whose names are listed in (*1*). We also thank members of the magnetometer, energetic particle, and ultraviolet teams on Mariner 10 for extensive discussions and comparisons of experimental results. We are grateful to E. W. Greenstadt for discussions concerning the nature of pulsating shocks, to V. Vasyliunas for discussions of spacecraft charging, and to M. Acuña for assistance in calibration, and to W. C. Feldman for helpful discussions.

29 May 1974

Magnetic Field Observations near Mercury: Preliminary Results from Mariner 10

Abstract. *Results are presented from a preliminary analysis of data obtained near Mercury on 29 March 1974 by the NASA-GSFC magnetic field experiment on Mariner 10. Rather unexpectedly, a very well-developed, detached bow shock wave, which develops as the super-Alfvénic solar wind interacts with the planet, has been observed. In addition, a magnetosphere-like region, with maximum field strength of 98 gammas at closest approach (704 kilometers altitude), has been observed, contained within boundaries similar to the terrestrial magnetopause. The obstacle deflecting the solar wind flow is global in size, but the origin of the enhanced magnetic field has not yet been uniquely established. The field may be intrinsic to the planet and distorted by interaction with the solar wind. It may also be associated with a complex induction process whereby the planetary interior-atmosphere-ionosphere interacts with the solar wind flow to generate the observed field by a dynamo action. The complete body of data favors the preliminary conclusion that Mercury has an intrinsic magnetic field. If this is correct, it represents a major scientific discovery in planetary magnetism and will have considerable impact on studies of the origin of the solar system.*

Results from a preliminary analysis of "quick-look" data obtained by the NASA-GSFC magnetic field experiment during Mercury encounter on 29 March 1974 are summarized in this report. The purpose of this investigation was to study the magnetic field environment of the planet Mercury and the nature of the solar wind interaction with it. There is substantial evidence in this initial assessment of the results to support the preliminary conclusion that an intrinsic planetary magnetic field exists. Rather unexpectedly, a very well-developed, strong, detached bow shock wave was observed, as well as a magnetosphere-like region in which the field magnitude increased to 98γ at closest approach, 704 km from the planetary surface. This is a factor of 5 greater than the average interplanetary magnetic field strength of 18γ measured outside the Mercurian bow shock.

Scientific interest in Mercury received a major stimulus in 1965 from data provided by radar observations of the planet. It was discovered (*1*) that the planet's rate of rotation was not synchronous with its orbital motion. Explanations for this remarkable result were soon forthcoming (*2*), and a new era in planetary studies began in which coupling of orbital motion and rotation rates was found to be considerably more complex and informative than previously expected.

For some time, it has been acknowledged that Mercury is anomalous among the terrestrial planets, having a remarkably high average density of 5.6 g/cm^3 for its small radius of 2434 km (*3*). Studies of the planet's interior have been hampered both by the inadequacy of available data concerning its shape, size, and mass and by the absence of definitive information concerning its rotational axis and precessional motion. Only recently have attempts been made to study these problems and their significance in the history of the formation of Mercury (*4*).

The atmosphere of Mercury has also been the subject of considerable speculation (*5*), the earlier work being prejudiced by the erroneous assumption of synchronous rotational and orbital periods. Studies incorporating new radar results (*6*) suggested that revision of the traditional concept of a planet devoid of an atmosphere was necessary.

In the absence of any evidence for appreciable rotation of the planet or for a substantial atmosphere, it was thought that Mercury would resemble our own moon in many respects. Taking into account recent observations of microwave emissions and the newly established correct rotation period for the planet, it was suggested strongly that its surface thermophysical characteristics would be rather close to those of the moon (*7*). There was no evidence for any radio emissions from Mercury such as those from Jupiter's radiation belts.

Thus, with the traditional view of geomagneticians that a rapidly rotating planet with some precession were features essential for generation of a planetary magnetic field (*8*), there was little reason to suggest an intrinsic field of Mercury. Some elementary estimates of a planetary magnetic field were made by using simple scaling laws for planetary volumes or rotation rates, or both, but the bases for these studies were rather speculative.

In specific studies related to the solar wind interaction with Mercury, the results depended on the planet's physical characteristics. Figure 1 summarizes four modes of interaction, of which three have been observed in the exploration of the solar system. In model A, a lunar type of interaction

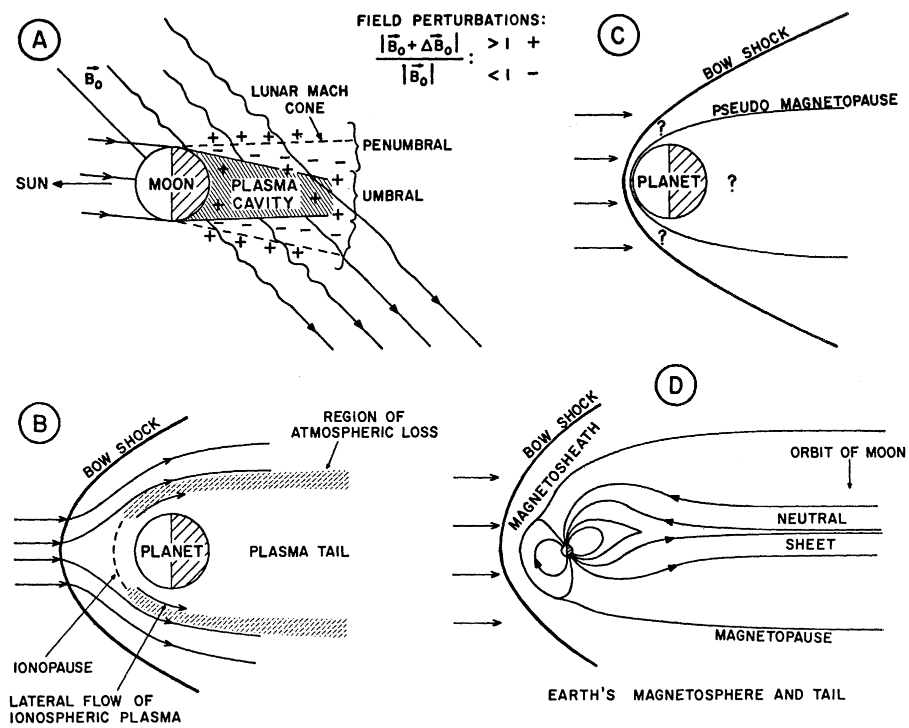

Fig. 1. Four models of the solar wind interaction with an object of planetary size. The weakest interaction, model A, is typified by the moon and occurs in the case of an insufficient intrinsic magnetic field or atmosphere and ionosphere to deflect the solar wind (*9*). In all other models a bow shock develops because of the deflection of super-Alfvénic flow around the planet. The deflection is due to a sufficient atmosphere and ionosphere in model B (*10*); a sufficiently conducting planetary interior in model C; or a sufficient intrinsic planetary magnetic field, as in the case of the earth, in model D.

was proposed (*9*), based on an atmosphere-ionosphere insufficient to deflect the solar wind flow and a planetary interior with electrical conductivity insufficient for induction of a significant secondary magnetic field. In model B, a modest atmosphere-ionosphere was proposed (*10*) and a deflected solar wind flow anticipated, contingent on the specific model of the atmosphere assumed. In this model there was no discussion of the magnetic field in the vicinity of the planet associated with the complex interaction with the magnetized solar wind.

Basic concepts of the induction of a secondary magnetic field were developed in association with studies of the solar wind interaction with the moon (*11*). The secondary magnetic field could be either a steady state field induced by the convective flow of the magnetized solar wind past the planet or a transient field associated with changes in the interplanetary magnetic field as observed at the planet. In the case of the moon, the low electrical conductivity of the surface layer decouples the planet from the solar wind for the steady state interaction mode and only the transient mode of induction is significant. Model C depicts, very qualitatively, a steady state induction mode; the question marks indicate regions where there are critical uncertainties regarding the interaction process and magnetic field topology.

Most authors have assumed that Mercury does not possess a sufficient magnetic field for deflection of solar wind flow. However, for completeness in this discussion and because of the results obtained, we include the solar wind interaction with the earth's magnetic field, model D. Here a substantial magnetosphere is developed which contains permanently trapped energetic particles forming the radiation belts and includes a very well-developed, large magnetic tail extending far downstream away from the sun, much like a comet tail.

Instrumentation. The magnetic field experiment consists of two triaxial fluxgate magnetometers. The dual magnetometer system used on Mariner 10 and its performance characteristics have already been described with the Venus encounter results (*12*). During Mercury encounter, the instrument operated continuously in the high range with each axis covering $\pm 128\gamma$. Vector measurements at intervals of 40 msec with 10-bit precision yielded quantization step sizes of 0.26γ. The root-mean-square noise level of each sensor over the band pass of 0 to 12.5 hertz ranged between 0.03 and 0.06γ, significantly less than the digitization value.

We shall not discuss the instrument further except to remark that, as the spacecraft passed through solar occultation at Mercury, no significant change in the spacecraft magnetic field was noted. This provides experimental in-flight verification of the assumption that the magnetic field of the spacecraft solar array panels was negligible. This solar array feature was designed by appropriate backwiring and tested before the flight, but was not checked at Venus encounter since no solar occultation occurred there. During Mercury encounter, a variable spacecraft magnetic field was observed with a maximum strength of 4γ at the outboard magnetometer.

At this early date, the accuracy of the measurements, combining all sources of error, is estimated to be approximately $\pm 1\gamma$ on each axis. The nature of the results and the magnitude of the fields measured are such that this is not a source of significant error in this preliminary report.

Mercury encounter observations. The trajectory of Mariner 10 during Mercury encounter was uniquely well designed for a study of the planetary magnetic field and solar wind interaction. The spacecraft path was approximately perpendicular to the planet-sun line on the dark side of the planet, very close to the antisolar point. See Fig. 2 for a presentation of the trajectory in Mercury-centered solar ecliptic (SE) coordinates. As is readily evident, the spacecraft moved rapidly past the planet, the relative velocity being 11 km/sec. Thus, accurate information relating the time of data acquisition to the time when Mariner 10 was at a particular position relative to the planet is very important.

Magnetic field observations during a 2-hour time interval surrounding closest approach are shown in Fig. 3. The format for presentation incorporates 6-second averaging periods for each orthogonal component of the magnetic field and a reconstituted average vector represented by a field intensity $\overline{F}$ at latitude θ and longitude ϕ in SE coordinates. The RMS parameter, which is invariant with respect to coordinate system, is sensitive to fluctuations on the time scale of tens of seconds or less.

Shortly after closest approach, the spacecraft passed into a period of radio occultation during which data were stored on a spacecraft magnetic tape recorder for subsequent retransmission. Special processing at Jet Propulsion Laboratory, Pasadena, California, has made available to us quick-look data tapes for both the real time data and the playback data at encounter.

As Mariner 10 approached the planet, the interplanetary magnetic field was slightly disturbed relative to observations made several days previously, as measured by the RMS value and as noted in the variable average field magnitude and direction. The magnitude was $18 \pm 2\gamma$, only slightly lower than expected from an extrapolation of the average magnetic field of 6γ observed at 1 A.U. to the Mercury encounter heliocentric distance of 0.46 A.U. The well-known formulas for the Archimedean spiral magnetic field embedded in the interplanetary medium predict a field magnitude of 22γ at a solar azimuthal angle ϕ of 155° or 335° for a solar wind velocity of 400 km/sec.

As can be seen from the data in Fig. 3, there are significant discontinuous changes in the magnetic field in the vicinity of Mercury. These cannot be interpreted in terms of a variable interplanetary magnetic field being swept past the spacecraft. The figure includes identification of both inbound and outbound bow shock crossings as well as apparent magnetopause traversals. The interpretation of these phenomena is based on our understanding of the bow shock and magnetopause observed in the terrestrial case. The character of the magnetic field observations is immediately reminiscent of observations obtained with a spacecraft traversing the earth's magnetosphere on the dark side at a distance of approximately 8 to 12 earth radii.

The very sharp change in magnetic field strength to values greater than 40γ noted at 2027 to 2028 U.T. (universal time) represents the inbound crossing of the Mercurian bow shock. In fact, three crossings occur during this time interval. The jump characteristics of the magnetic field at the bow shock are discussed below in a presentation of the more detailed data. Subsequently, the spacecraft is immersed in a sheath or boundary layer in which a disturbed magnetic field regime exists. As the spacecraft continues along the trajectory, the field magnitude decreases steadily to 30γ in a manner characteristic of a steady state magnetosheath. Mariner 10 again traverses a sharp boundary at 2037 U.T. at which the magnitude of the field increases to more than 40γ, while the fluctuations decrease significantly. Most importantly, the direction of the magnetic field simultaneously changes abruptly by 135° (see plot of ϕ in Fig. 3). The magnetic field then increases steadily up to the maximum of 98γ near closest approach at 2047 U.T. The direction of the magnetic field is mainly parallel to the Mercury-sun line with a polarity sense away from the planet. There is also a smooth

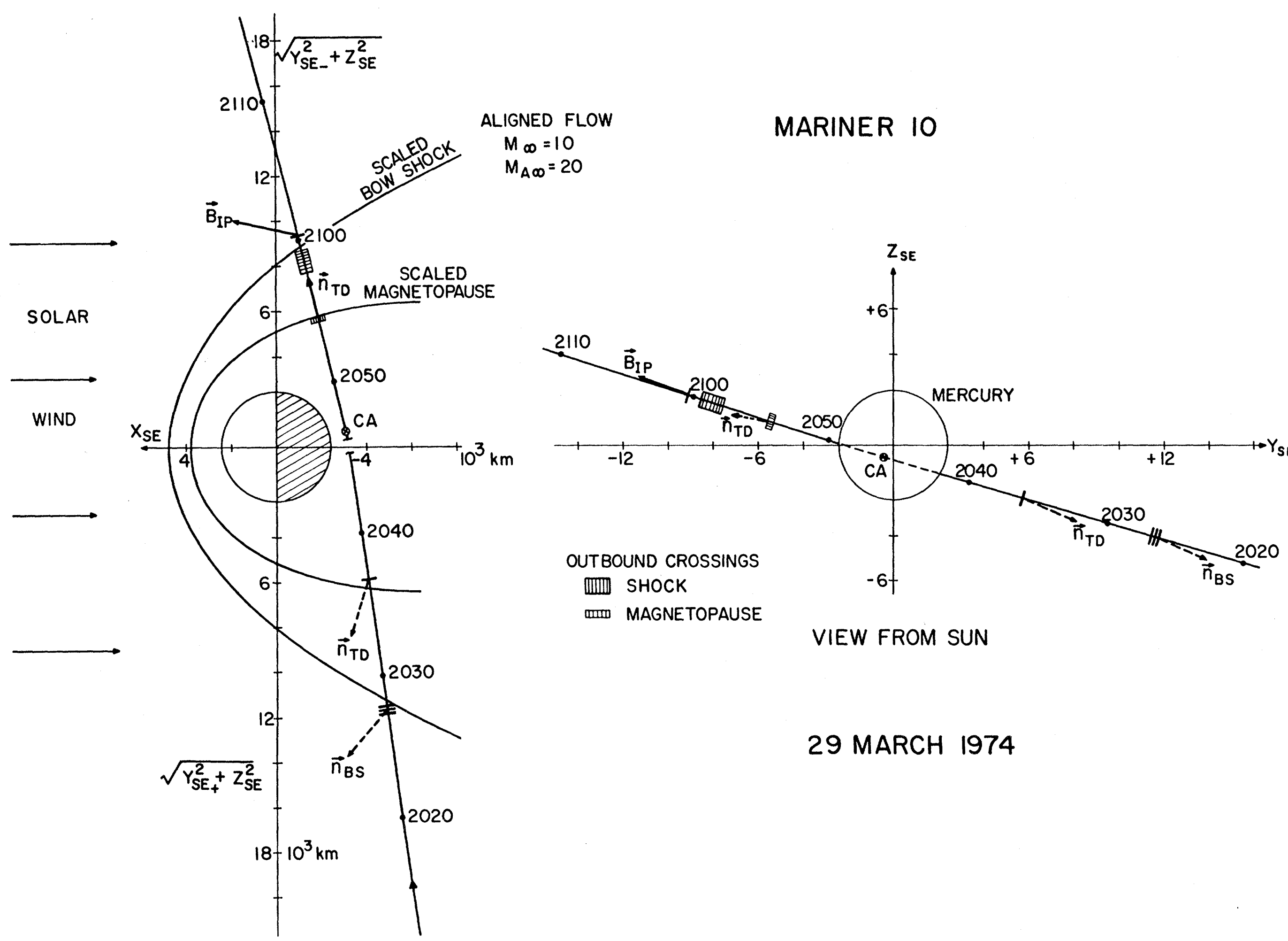

Fig. 2. Encounter trajectory of Mariner 10 in Mercury-centered solar ecliptic (SE) coordinates ($+X_{SE}$ axis toward the sun, Z_{SE} axis perpendicular to the ecliptic, and Y_{SE} axis completing a right-handed coordinate system). (Left). Plot of the distance from the X_{SE} axis as ordinate; (right) true projection of the trajectory as viewed from the sun. For other abbreviations see Fig. 3 and text.

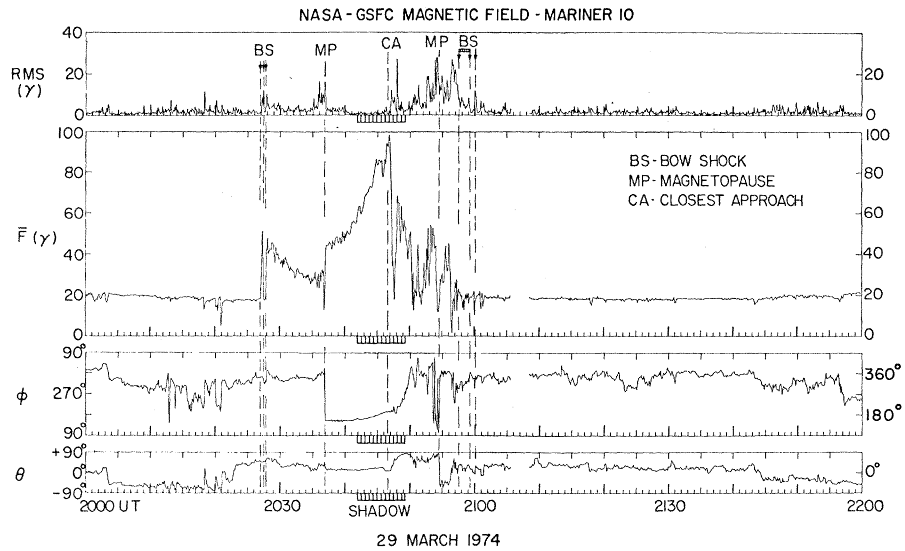

Fig. 3. Magnetic field data averaged for 6-second periods during Mercury encounter in spacecraft-centered solar ecliptic coordinates. The latitude of the magnetic field vector is represented by θ and the longitude by ϕ; the field intensity is $\overline{F}$, and RMS represents the Pythagorean mean of the root-mean-square deviations in the X, Y, and Z components computed during the 6-second periods. Significant discontinuities observed in the magnetic field data are identified.

but small variation in the orientation of the field throughout this time period.

Following closest approach, there occurred a distinct change in the character of the magnetic field. Large-amplitude variations over a wide range of time scales are observed. A large field depression with a minimum of 17γ occurs precipitously just after closest approach, with the field magnitude rising back soon afterward to 70γ. Subsequently, the field magnitude varies considerably, while the direction steadily changes to point northward relative to the ecliptic. The considerable variability in the field magnitude is not accompanied by a comparable variability in field direction.

Between 2054 and 2055 U.T. the magnetopause is crossed outbound, although it is a less distinct crossing and the field directional change is primarily a change from northward to southward. As the spacecraft continues on in the sheath, it encounters magnetic fields highly variable in both direction and magnitude, and the bow shock crossing is not readily apparent in this format.

The detailed 40-msec data, to be presented shortly, indicate that the outbound bow shock crossing (or crossings) occurred somewhere between 2057 and 2059 U.T. within the region indicated in Fig. 3. This bow shock crossing is similar to that observed by Mariner 10 during Venus encounter (*12*) in which there was no abrupt and distinctive jump. This is probably associated with the relative geometry of the upstream interplanetary magnetic field and the shock surface. When the interplanetary field direction is closely aligned with the shock surface normal, the shock is referred to as parallel. Under such circumstances, large-amplitude fluctuations are known to occur from studies of the earth's bow shock (*13*). This type of pulsation bow shock occurs moderately often on the dawn side of the earth's bow shock because of the Archimedean spiral geometry of the interplanetary magnetic field.

More detailed presentations of subsets of the data are given in Figs. 4 and 5. In addition to F, θ, and ϕ describing the instantaneous vector measurements at 40-msec intervals, the X, Y, and Z SE components are also presented. The clear and distinctive appearance of high-frequency fluctuations just outside the inbound bow shock is evident in Fig. 4A. That three crossings occurred is interpreted as representing relative motion of the bow shock across the spacecraft due to moderate changes in the upstream interplanetary medium and the response of the Mercurian bow shock configuration. The nature of the fluctuations in the sheath region is seen to be rather different. High frequencies are observed outside (that is, upstream from the bow shock) while relatively lower frequencies are observed in the sheath (downstream).

Inside the magnetopause, the field is very steady and any fluctuations are very small. This character of the magnetic field is continued through to the maximum field period shown in Fig. 4C. Small sinusoidal perturbations of the magnetic field, analogous to micropulsations observed terrestrially, occur between 2045 and 2046 U.T. However, these detailed data in the magnetosphere-like region show that the field magnitude is extremely steady and give no indication that any of the variability of the interplanetary magnetic field or the sheath region has been transmitted into this region of the Mercurian magnetosphere. This segment of the data reflects what is ideally expected from observations obtained while traversing any planetary obstacle on its dark side if the planet possesses a magnetic field sufficiently strong to deflect the solar wind and lead to the development of a detached bow shock wave.

Details from the outbound magnetopause and bow shock crossings are shown in Fig. 5. The magnetopause is identified at 2054 U.T. by the abrupt change in the latitude angle θ from northward to southward. This is followed by a period of relatively rapidly alternating sign, seen for approximately 40 seconds. This is believed to reflect the relative motion of the magnetopause and the variability of the magnetospheric structure, probably due to variations in the interplanetary medium and the response of the Mercurian environment to these fluctuations. It may also reflect the close proximity of the spacecraft to a neutral sheet–field reversal region such as is found in the earth's magnetic tail. The sheath region is again well defined by relatively larger amplitude fluctuations of all three field components.

With the better time resolution, the bow shock is now somewhat more distinctive. The fluctuations change from relatively lower frequencies and larger amplitudes to higher frequencies and smaller amplitudes. The period of bow shock crossings is extended, however, from 2057 to 2059 U.T., with a more distant bow shock crossing apparently observed just after 2100 U.T.

The identification of the time of occurrence of these various boundaries is important in determining the relative positions of the solar wind obstacle boundary, the magnetopause, and the detached bow shock. The identified positions of the boundaries are superimposed on the trajectory plot of Fig. 2 with uncertainties indicated accordingly. Also included are two curves representing a scaled magnetopause and bow shock, both obtained from theoretical studies of the solar wind interaction with the geomagnetic field. The shape of the magnetopause shown (*14*) is computed for the case of the solar wind incident on a Mercury-centered magnetic dipole orthogonal to the solar wind flow (assumed along $-X_{SE}$) and the plane of the figure. The bow shock shown (*15*) is scaled according to a sonic Mach number (M_x) of 10 and Alfvén Mach number (M_{Ax}) of 20 at the subsolar point. These values correspond approximately to the measured values of the interplanetary magnetic field, plasma density, and velocity. The theoretical bow shock position presented here is for the only solvable case so far in magnetohydrodynamics, that of aligned flow, in which the upstream magnetic field and solar wind velocity are parallel. Since it is assumed that the apparent solar wind direction is parallel to the Mercury-sun line, this implies a true flow from 3.7°E, when the effect of aberration due to planetary heliocentric orbital motion is allowed for.

No direct attempt has been made to adjust the scaled curves to exactly fit all observed boundary traversals. But the comparison with the observed boundary positions is remarkably good, considering the normal variability of the solar wind and its concomitant effects.

For this fit, the value of the stagnation point distance (*14*)

$$r_{sp} = 1.07\left[\frac{M^2}{4\pi mnV^2}\right]^{1/6}$$

has been assumed equal to 1.6 Mercury radii (R_M) ($R_M = 2434$ km). (Here M is the magnetic moment, m the proton mass, n the plasma density, and V the solar wind velocity.) With the measured value of $n = 17$ particles per cubic centimeter and the estimate of $V = 600 \pm 50$ km/sec, M is determined to be $380 \pm 32\gamma\ R_M^3$.

Analysis of boundary crossings. The relative position of the bow shock and magnetopause boundaries is important in determining the geometry of the obstacle to solar wind flow. In order to obtain accurate estimates of the appropriateness of the fit of the bow shock and magnetopause boundaries, normal vectors to these surfaces have been calculated where possible. They are valuable since they augment the discrete point location by permitting extrapolation of the surface shape beyond the point of observation. This is analogous to a classical boundary value problem in which one has information that fixes the slope as well as the magnitude of a quantity of interest at a specific boundary.

The inbound bow shock was first observed at 2027:20 U.T., immediately followed by another crossing, which appears as a reverse shock, and finally the third and last crossing at 2027:50 U.T. Average magnetic field quantities were used in estimating the shock normal. An analysis interval of 84 seconds immediately preceding the first crossing and another interval of 84 seconds after the last crossing were used. It is implicitly assumed that the interplanetary magnetic field is stationary during 3½ minutes. The preshock and postshock field averages in standard X, Y, Z SE coordinates, normalized to unity, and their respective magnitudes were found to be

$$\hat{B}_{pre} = (0.630, -0.237, 0.740)$$
$$|\bar{B}|_{pre} = 17.3\gamma$$

and

$$\hat{B}_{post} = (0.497, -0.119, 0.860)$$
$$|\bar{B}|_{post} = 40.3\gamma$$

Hence, the field magnitude jump ratio was 2.3 and the angle between the preshock and postshock field vectors was 12°, implying that the field vectors were almost parallel. Under this condition, the shock normal cannot be cal-

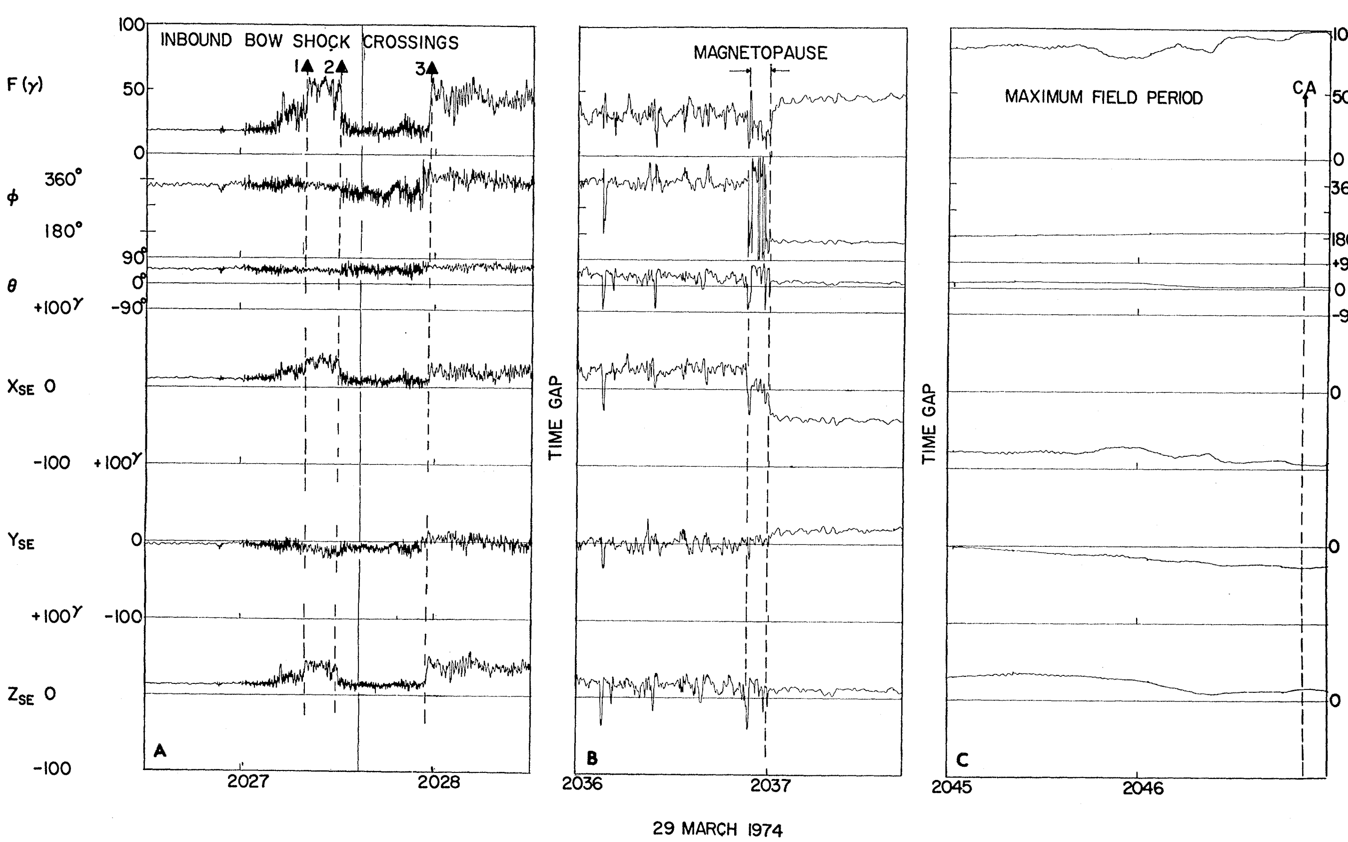

Fig. 4. Detailed magnetic field data taken with an instrument sampling rate of 25 hertz during the inbound bow shock and magnetopause crossings and near closest approach (*CA*). The three orthogonal components are presented in the bottom three traces.

culated by using the magnetic coplanarity theorem (*16*) because of an unacceptable magnification of errors (*17*). Since data for the ion component of the plasma were not available, a more sophisticated method of least squares fitting to the shock conservation equations was not possible either (*17*).

However, the data show that the shock character was typically that of an approximately perpendicular type (that is, the shock surface normal is perpendicular to the upstream field). Thus, this was assumed as was the cylindrical symmetry of the bow shock surface about an axis parallel to the X axis. With knowledge of the spacecraft position at the crossing, this is sufficient to yield an accurate estimate of the bow shock normal

$$\hat{n}_{\mathrm{BS}} = (0.65,\ 0.70,\ -0.30)$$

This corresponds to longitude $\phi = 47°$ and latitude $\theta = -18°$, while the angle between the bow shock normal and the X axis is 50°. The angle between the projection of the bow shock normal onto the YZ plane and the Y axis is found to be $-23°$. Figure 2 shows the bow shock normal in terms of the relevant angles.

Using the upstream field magnitude of 17γ and the plasma density of $n =$ 17 particles per cubic centimeter from the Mariner 10 plasma science experiment, we compute the upstream Alfvén speed to be $V_A = 90$ km/sec. Assuming that the protons behave according to the relation between plasma bulk velocity and temperature valid at 1 A.U. (*18*), we calculate the sound speed to be $V_s = 60$ km/sec. The component of the upstream plasma bulk speed along the bow shock normal is 390 ± 42 km/sec, with 600 ± 50 km/sec as the value for the solar wind speed. Hence, the upstream fast mode Mach number is 3.6 ± 0.3 and the sonic Mach number is 6.5 ± 0.5. This yields good agreement with the magnitude of the field jump ratio of 2.3 (*19*).

The inbound crossing of the obstacle to solar wind flow was assumed to be a classical magnetohydrodynamic tangential discontinuity (TD) (*16, 20*), across which no plasma flow takes place and perpendicular to which no magnetic field exists. Hence, using the magnetic field data alone, we computed a normal to this boundary observed at 2036:50 U.T. with 84-second averages for precrossing and postcrossing observations. This yields a normal of

$$\hat{n}_{\mathrm{TD}} = (0.30,\ 0.88,\ -0.36)$$

The angular coordinates of this normal are longitude $\phi = 72°$ and latitude $\theta = -21°$. Accordingly, the angle with respect to the X axis is 73° and the angle to the Y axis in the YZ plane is $-22°$. The field magnitude jump ratio across this boundary was 1.6. Such a tangential discontinuity is expected at a classical magnetopause boundary crossing. It is often the case for the terrestrial magnetopause.

A similar calculation has been done for the outbound crossing of the obstacle boundary, which occurred at 2054:15 U.T. For the analysis 42-second intervals were used to obtain preboundary and postboundary averages; a 42-second interval including the crossing was omitted because of the high RMS values of the components. From these data, the normal to the tangential discontinuity on the outbound crossing is

$$\hat{n}_{\mathrm{TD}} = (0.26,\ -0.94,\ 0.21)$$

The longitude $\phi = 285°$ and latitude $\theta = 13°$. Accordingly, the angle with respect to the X axis is 75° and the angle to the Y axis in the YZ plane is 13°. The normal is not as accurately determined for the outbound crossing as for the inbound crossing because of the greater fluctuations of the magnetic field near the outbound obstacle boundary.

The outbound bow shock crossing, occurring between 2057 and 2059 U.T. and briefly at 2100 U.T., appears to be a multiple crossing of a pulsation shock. This occurs, as previously mentioned, when the shock is of the parallel type, that is, when the field direction

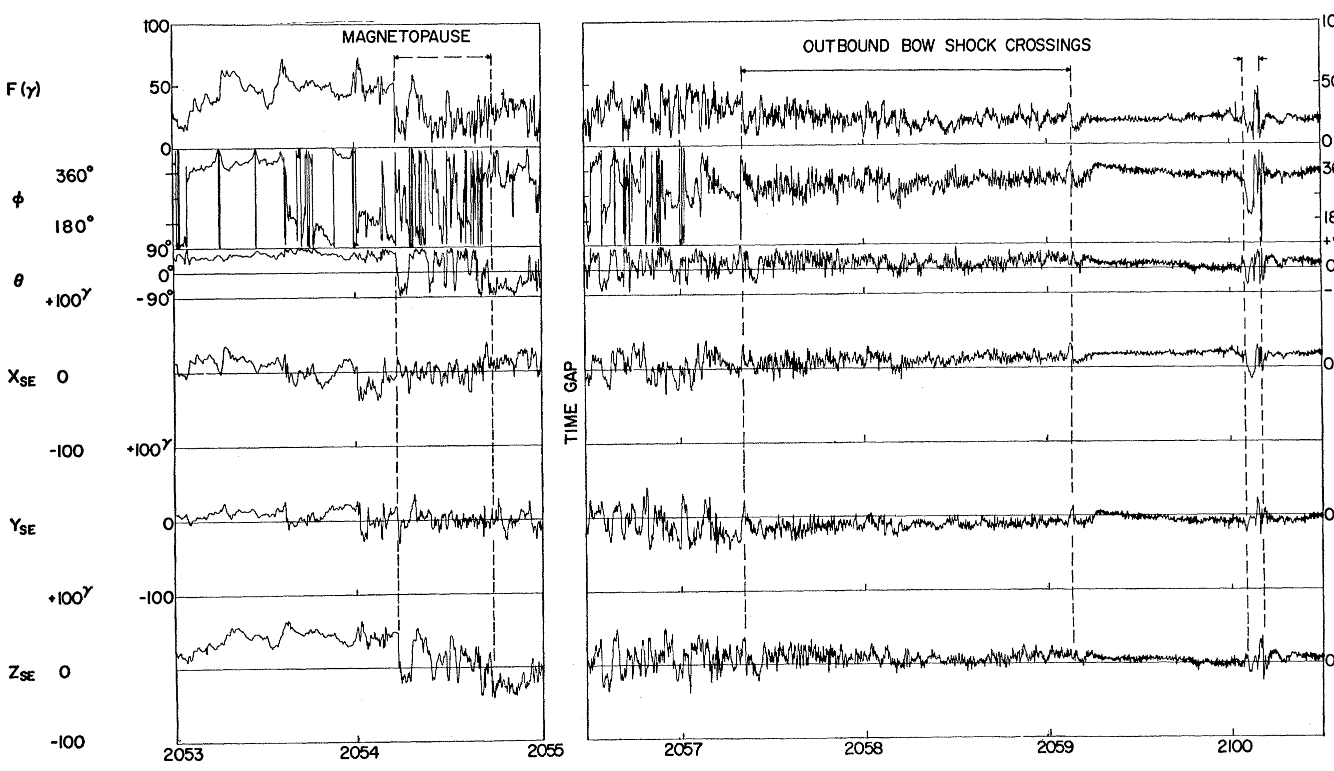

Fig. 5. Detailed magnetic field data taken during the outbound magnetopause and bow shock crossings.

and shock normal are aligned with each other (*13*).

Figure 2 shows the projections of the tangential discontinuity normals on the trajectory. In addition, the solid lines in Fig. 2 correspond to theoretical boundary positions, as discussed above. There is remarkably good agreement between the computed normals and the calculated boundary positions. This agreement between extrapolated surfaces determined from the normals computed at the boundary crossings and the boundary positions themselves leads us to conclude that the obstacle to solar wind flow is global in size. That is, it is not plausible to expect that a trailing shock such as a limb shock, due to the deflection of the solar wind near the terminators of the flow, would lead to the geometrical configuration and the shock strength measured by the Mach number which are required by these magnetic field data.

It should be noted that both the identification of the time of occurrence of these boundaries (bow shock and magnetopause) and the nature of their signatures (abrupt or diffuse) are in excellent agreement with the results of the plasma science experiment on Mariner 10.

Interpretation of the origin of the magnetic field. The origin of the interplanetary magnetic field upstream of either the bow shock or the magnetopause is the solar magnetic field. Within the magnetopause boundaries, the field is the vector sum of secondary magnetic fields associated with the solar wind interaction and any intrinsic planetary magnetic field.

There is no unique characteristic of the data that makes it possible to separate the internal and external contributions, since the data are only for a very restricted region of space along the spacecraft trajectory. If magnetic field data were available over a closed surface enclosing the planet, it would be possible to separate the internal and external sources by using classical methods of mathematical analysis (*21*).

Thus, in our preliminary interpretation, we have considered the simple model of an offset, tilted dipole as representing the intrinsic field of the planet. Further, we have assumed that this represents the major contribution of the observed magnetic field only during the interval from 2041 to 2050 U.T., surrounding closest approach, when the spacecraft is within 2400 km of the planetary surface. By using selected data from this interval and minimizing the mean-square fit of the assumed dipole, we obtain a result whose fit to the data is illustrated in Fig. 6. The observed and theoretical orthogonal magnetic field components are presented, and a reasonably good fit is obtained. Discrepancies, especially in the X component, may be due to the secondary magnetic fields associated with currents flowing on the magnetopause extending the planetary magnetic field out behind the planet to form a magnetic tail. While there are indications that the discrepancies after closest approach may be due to complex local fields on the planetary surface, they probably represent time variations of the structure of the Mercurian magnetosphere.

The coordinates and values of the dipole so determined are as follows: The position is offset 0.47 R_M at $\phi = 62°$ and $\theta = 17°$; the moment has magnitude $227\gamma\ R_M^3$ at $\phi = 209°$ and $\theta = -70°$. These preliminary values are uncertain, in a mathematical sense, by approximately 10 percent in offset distance, 20 percent in the magnitude of the dipole moment, and 10° in all direction angles.

This intrinsic magnetic dipole is oriented within 20° of the ecliptic pole, or almost aligned with the axis of rotation of the planet, considering that there is an uncertainty of some 10° in the planetary rotation axis. The large offset might appear at first to be anomalous. However, considering the very large core size (*22*) indicated by the anomalously high average density of the planet, it is quite acceptable.

A further implication of this dipole concerns the magnetic field configuration of the Mercurian magnetosphere. An isointensity map of the intrinsic magnetic field on the surface of the planet is presented in Fig. 7A. Also included are intersections of the magnetic poles and equator and the trace of the Mariner 10 subspacecraft point. The field at an altitude of 0.6 R_M (1460-km elevation) is presented in Fig. 7B. This is the appropriate distance for the stagnation point inferred in the previous section, when the interpretation of the obstacle boundary and bow shock position was made.

Immediately evident in these two isointensity contour maps is the asymmetry due to the dipole offset. The magnetosphere of Mercury is clearly not as symmetrical about the Mercury-sun line as the earth's is about the earth-sun line. However, it is plausible to assume that a magnetic tail and embedded neutral sheet–field reversal region will be developed on the dark side, similar to the earth's. Then the effect of the dipole offset and tilt would be to bring the neutral sheet region closer to the surface of the planet near the dawn terminator than at the dusk terminator at the time of encounter, 29 March 1974. The weaker fields and closer proximity to the magnetic equator, as Mariner 10 approached the outbound magnetopause, combine to yield a consistent image of the origin of the field as due to an intrinsic but modest magnetic field of the planet Mercury.

The offset of the dipole in the YZ plane will have an effect on the positions of the magnetopause and bow shock. However, there is some compensation due to the dipole tilt, so that the net effect may not lead to a significant inconsistency with the results illustrated in Fig. 2 where a centered dipole with no tilt was assumed. Similarly, the offset in the $+X$ direction, 0.21 R_M, compensates the lower moment determined, $227\gamma\ R_M^3$, relative to the value of $380\gamma\ R_M^3$ inferred only from the boundary positions. The stagnation point distance from the YZ plane is then found to be approximately 1.7 R_M, which compares favorably with the previously used value of 1.6 R_M, considering the uncertainty associated with the fitting of the theoretical bow shock and magnetopause surfaces to the observed crossings and normals.

Possibilities of induction mode. The steady state or unipolar induction mode is generated by the electrical field $\mathbf{E} = -\mathbf{V} \times \mathbf{B}$ associated with the solar wind convective transport of the interplanetary magnetic field $\mathbf{B}$ past the planet (*23*). The resulting electrical currents close in the solar wind, regardless of whether they are induced in the ionosphere or the planetary interior (*24*). For such a mode there must be direct electrical contact between the ionosphere or planetary surface and the solar wind. Thus, the solar wind cannot be completely deflected away from the ionosphere or the planet itself.

The observations by Mariner 10 of the Mercurian bow shock and magnetopause correspond to positions and characteristics which are not consistent with such a postulated geometry, where only a portion of the flow is deflected and this occurs very close to the planet. Also, the magnetic field topology as observed at the magnetopause is not consistent with the theoretical field configurations in which the magnetic field is draped around the planet *(24)*. A recent quantitative study of the steady state induction mode appropriate to the moon assumes complete absorption of the solar wind on the upstream hemisphere *(25)*. The magnetic field configuration obtained confirms the earlier qualitative studies *(24)* and does not show large directional changes at what would correspond to the magnetopause, which are clearly seen in the Mariner 10 data. Finally, no modest-sized magnetosphere-like region was observed at Venus *(12)*, the normalized stagnation point distance being only 1.025 whereas at Mercury it is ~ 1.6. These many considerations of boundary positions and inferred obstacle size, as well as the solar wind deflection, existence of a magnetosphere-like region, magnetic field topology, and comparative solar interaction studies, lead us to conclude that the unipolar steady state induction mode was not active at Mercury encounter.

The transient induction mode is generated by an implicit time variation of the interplanetary magnetic field as seen by the planet. This can be due to either an explicit time variation of the interplanetary magnetic field, $\partial \mathbf{B}/\partial t$, or a spatial variation, $\mathbf{V} \cdot \nabla \mathbf{B}$, due to the convection past the planet of a spatially varying interplanetary field. For this mode, electrical currents circulate completely within the planetary ionosphere or interior and no direct electrical contact with the solar wind is required. Again, the absence of a modest-sized magnetosphere at Venus during the extended period when such a feature could have been observed suggests that, even if a significant Mercurian ionosphere existed, the transient induction mode would not be active.

The quasi-static nature of the magnetic field observations during the inbound portion of the Mariner 10 trajectory at Mercury encounter implies that a magnetosphere-like region had existed on a time scale at least of the order of the time interval from inbound bow shock crossing to closest approach. This places a constraint on the minimum conductivity of the planetary interior since the characteristic time constant for decay of electrical currents in such a mode is given by

$$\tau = \frac{\mu_0 \sigma R_M^2}{\pi^2}$$

Assuming a magnetic permeability (μ_0) of free space and a uniformly conducting planet, we obtain a minimum conductivity (σ) of 10^{-4} mho per meter. This is not an unreasonable value for silicates at the elevated temperatures which must be appropriate in the Mercurian interior, and it is easily satisfied by any metal phases, although it depends very much on the detailed grain structure and intergrain electrical connections. However, the value is rather implausible for near-surface material, even at the subsolar point.

A model of a uniformly conducting planet is not a reasonable assumption, and a model of an insulating shell surrounding a conducting core requires a combination of higher magnetic permeability and conductivity. Neither of these two requirements create special problems for Mercury because its high aver-

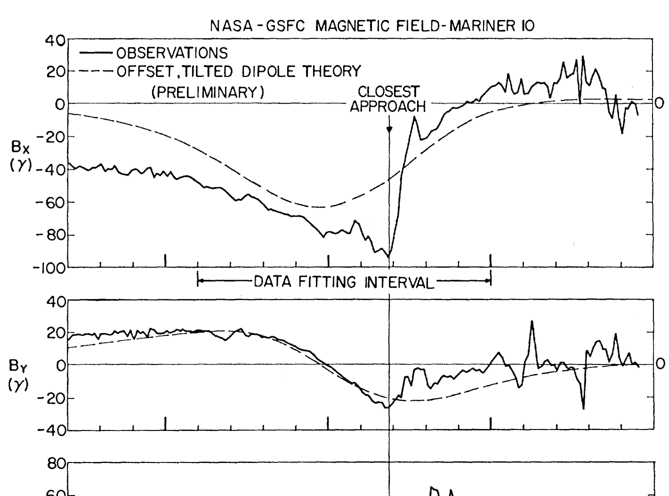

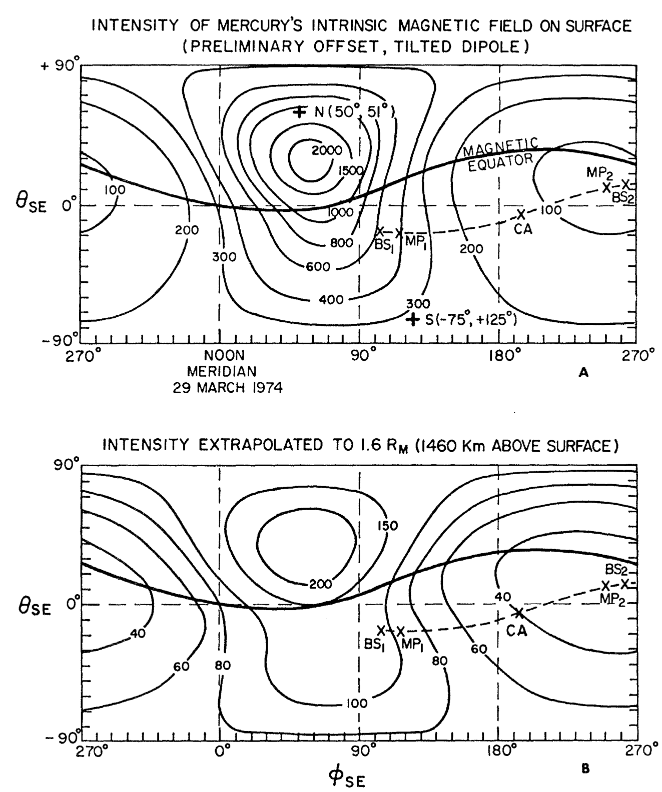

Fig. 6 (left). Comparison of observed and theoretical orthogonal components (B_X, B_Y, B_Z) of the magnetic field near closest approach. The observational data are averaged over 6-second periods. The theoretical planetary magnetic field is represented by an offset, tilted dipole chosen to best fit the data in a least-squares measure during the interval 2041 to 2050 U.T. (see text). Fig. 7 (right). Predicted isointensity contours and characteristics of an intrinsic magnetic field on the surface of Mercury (A) and at an elevation of 1460 km from the surface (B). The magnetic polarity is in the same sense as the earth's. The appreciable offset distorts the surface field so that it varies by more than an order of magnitude over the surface. The position of Mariner 10 during encounter trajectory and the associated bow shock (*BS*) and magnetopause (*MP*) crossings are indicated relative to the magnetic equator.

age density implies a substantial iron-rich core (*22*). Moreover, the secondary magnetic field which would develop in such a mode is dominated by a dipole term. Since there were significant, abrupt changes in the interplanetary magnetic field direction near 2020 U.T., we do not believe it possible at present to reject the possibility of an induction mode. However, it requires a unique combination of circumstances coincident with the time of encounter and also a very strong secondary field, much stronger than in the lunar case, in order that the obstacle be as large as has been inferred. We believe the most plausible explanation is the conclusion offered in the previous section, that Mercury has a modest intrinsic magnetic field.

Discussion. In the previous sections, arguments for the interpretation of the magnetic field observations in terms of a modest intrinsic planetary magnetic field have been presented. In the analysis yielding an offset, tilted dipole it was explicitly assumed that there were no time variations in the structure of the Mercurian magnetosphere during Mariner 10 observations. However, it should be noted that the characteristic change in magnetic field data from a tail-like configuration to a more dipole-like configuration following closest approach may be due to a temporal change in the Mercurian magnetospheric structure. By intercomparing these data with the plasma and particle measurements, it should be possible to clarify this possibility.

One effect of such a temporal variation on the interpretation would be that it could masquerade as a spatial variation of the magnetic field and lead to an erroneous conclusion regarding the magnitude of the dipole offset and tilt.

These results have significant implications regarding the present state and past history of formation of Mercury. The intrinsic planetary magnetic field may be due to a dynamo currently active within the planetary interior, or it may be a residual remanent magnetic field associated with a now extinct dynamo. Thus, it is possible that Mercury rotated faster earlier in its history than at present. On the other hand, if the transient induction mode is the source of the field, it places a constraint on the interior electrical conductivity.

Assuming that the intrinsic dipole interpretation is correct, we can reach some conclusions regarding the interaction of the solar wind with Mercury in its present state. The large offset and modest size of the dipole moment suggest that, under normal conditions, Mercury should not have a permanent trapped radiation belt. However, a magnetic tail should exist and should contain an embedded neutral sheet–field reversal region where particles are accelerated by field line merging.

Because the dipole is approximately perpendicular to the planet's orbital plane, the size of the Mercurian magnetosphere and tail would not change significantly during the Mercurian year. However, the distance of the stagnation point of solar wind flow relative to the subsolar point on the planetary surface would change considerably because of the large dipole offset. Because of the variation in the heliocentric distance of Mercury, the temporal variations in the solar wind momentum flux, and the changing value of the planetary field in the subsolar region, it should be possible for the solar wind to compress the planetary field to the surface. Thus, since the surface of the planet would not always be protected from the direct impact of solar wind flux, the optical properties of the planet's surface in certain regions should reflect the effects of proton bombardment characteristically observed on the lunar surface.

If Mercury also has a weak atmosphere, then acceleration of particles in the neutral sheet might lead to precipitation of particles into the polar regions and to "auroral" events. Direct access of particles from the interplanetary medium to the polar region is always possible.

These are speculative remarks, but represent logical conclusions based on the existence of an intrinsic Mercurian magnetic field. We once again emphasize the preliminary nature of the interpretation. The offset, tilted dipole result inferred in this first analysis should not be taken as more than a logical and simplified starting point for studying what is certainly a complex interactive process. We interpret these results, however, as strongly suggesting that an intrinsic field does indeed exist. Final confirmation of this conclusion will be possible if another appropriately configured Mercury encounter takes place. Unfortunately, the second encounter by Mariner 10 will not satisfy this requirement and it is not expected therefore to contribute any additional useful data to these investigations.

Conclusions. Direct observations of the magnetic field environment of Mercury by the magnetic experiment on Mariner 10 show the presence of a well-developed bow shock wave and magnetosphere region. A fundamental question not yet uniquely resolved is whether the magnetic field observations are consistent with an intrinsic planetary magnetic field or with a field induced by solar wind interaction. Considering the well-studied solar wind interaction with the moon and the recent Mariner 10 observations at Venus, it appears that the magnetic field data are not consistent with the steady state induction mode of interaction but may be consistent with the transient mode.

The modest size of the apparent magnetosphere of Mercury precludes a determination of an assumed intrinsic magnetic moment with high confidence. Preliminary analysis of a restricted data set obtained near closest approach yields an offset tilted dipole whose parameters are generally consistent with other aspects of the data. The moment's magnitude is $227\gamma\ R_M{}^3$, which is 4.1×10^{-4} that of the earth's dipole moment. Whereas the dipole's offset, 0.47 R_M, is significant, the tilt is within 20° of the ecliptic pole. This is probably close to the planetary rotation axis, itself uncertain to 10°. With the anomalously high average density of this small terrestrial planet, such a large dipole offset is not implausible. It should be noted, however, that temporal variations of the structure of the magnetosphere of Mercury would masquerade as spatial variations of the magnetic field in the interpretation of data from a single flyby encounter.

If the interpretation of an intrinsic planetary magnetic field at Mercury is validated by future studies and additional observations, it will represent a substantial discovery in the exploration of the solar system and will contribute significantly to the study of its origin.

N. F. Ness
K. W. Behannon
R. P. Lepping
NASA–Goddard Space Flight Center, Greenbelt, Maryland 20771
Y. C. Whang
Catholic University of America, Washington, D.C. 20017
K. H. Schatten
Victoria University, Wellington, New Zealand

References and Notes

1. G. H. Pettengill and R. B. Dyce, *Nature* (*Lond.*) **206**, 1240 (1965).
2. G. Columbo, *ibid.* **208**, 575 (1965); P. Goldreich and S. Peale, *Astron. J.* **71**, 425 (1966); G. Columbo and I. I. Shapiro, *Astrophys. J.* **145**, 296 (1966).
3. G. P. Kuiper, *Commun. Lunar Planet. Lab.* **143**, 165 (1970).
4. S. J. Peale, *Icarus* **17**, 168 (1972); *Astron. J.*, in press.
5. G. Field, in *The Origin and Evolution of the Atmospheres and Oceans*, P. J. Brancazio and A. G. W. Cameron, Eds. (Wiley, New York, 1964).
6. S. I. Rasool, S. H. Gross, W. E. McGovern, *Space Sci. Rev.* **5**, 565 (1966).
7. D. Morrison and C. Sagan, *Astrophys. J.* **150**, 1105 (1967); D. Morrison, *Space Sci. Rev.* **11**, 271 (1970).
8. W. Elsasser, *Phys. Rev.* **9**, 106 (19 E. C. Bullard and H. Gellman, *Philos. Trans. R. Soc. Lond. Ser. A Math. Phys. Sci.* **247**, 213 (1954); W. V. R. Malkus, *Science* **160**, 259 (1968); D. Gubbins, *Rev. Geophys. Space Phys.* **12**, 137 (1974).
9. N. F. Ness and Y. C. Whang, *J. Geophys. Res.* **76**, 3136 (1971).
10. P. M. Banks, H. E. Johnson, W. I. Axford, *Comments Astrophys. Space Phys.* **2**, 214 (1970).
11. C. P. Sonett and D. S. Colburn, *Phys. Earth Planet. Interiors* **1**, 326 (1968); J. L. Blank and W. Sill, *J. Geophys. Res.* **74**, 736 (1969); G. Schubert and K. Schwartz, *Moon* **1**, 106 (1969).
12. N. F. Ness, K. W. Behannon, R. P. Lepping, Y. C. Whang, K. H. Schatten, *Science* **183**, 1301 (1974).
13. E. W. Greenstadt, I. M. Green, G. T. Inouye, D. S. Colburn, J. H. Binsack, E. F. Lyon, *Cosmic Electrodyn.* **1**, 160, 279, and 316 (1970); E. W. Greenstadt, *J. Geophys. Res.* **77**, 1729 and 5467 (1972); T. G. Northrop and T. J. Birmingham, *ibid.* **78**, 2308 (1973).
14. J. Y. Choe, D. B. Beard, E. C. Sullivan, *Planet. Space Sci.* **21**, 485 (1973).
15. A. W. Rizzi, thesis, Stanford University (1971).
16. D. C. Colburn and C. P. Sonett, *Space Sci. Rev.* **5**, 439 (1966).
17. J. K. Chao, *MIT Report CSR TR-70-3* (1970); R. P. Lepping and P. D. Argentiero, *J. Geophys. Res.* **76**, 4349 (1971).
18. L. F. Burlaga and K. W. Oglivie, *Astrophys. J.* **159**, 659 (1970).
19. G. R. Smit, *ESRO Report SN-17* (European Space Research Institute, Frascati, Italy, 1967); B. Bavassano, F. Mariani, U. Villante, N. F. Ness, *J. Geophys. Res.* **76**, 5970 (1971); *ibid.* **77**, 2004 (1972).
20. L. F. Burlaga and N. F. Ness, *Solar Phys.* **9**, 467 (1969); D. M. Willis, *Rev. Geophys. Space Phys.* **9**, 953 (1971).
21. S. Chapman and J. Bartels, *Geomagnetism* (Clarendon, Oxford, 1940).
22. S. Plagemann, *J. Geophys. Res.* **70**, 985 (1965); R. A. Lyttleton, *Astrophys. Space Sci.* **5**, 18 (1969).
23. D. S. Colburn, C. P. Sonett, K. Schwartz, *Earth Planet. Sci. Lett.* **14**, 325 (1972).
24. A. J. Dessler, in *Atmospheres of Venus and Mars*, J. C. Brandt and M. B. McElroy, Eds. (Gordon & Breach, New York, 1968), p. 241; F. S. Johnson and J. E. Midgeley, *Space Res.* **9**, 760 (1969); F. C. Michel, *Rev. Geophys. Space Sci.* **9**, 427 (1971); J. L. Blank and W. R. Sill, *Bellcomm. TM 72-2015-1* (1972); P. A. Cloutier and R. E. Daniell, *Planet. Space Sci.* **21**, 463 (1973).
25. G. Schubert, and B. Horning, in preparation.

26. We appreciate discussions of these results with our colleagues from the plasma science experiment and charged particle experiment teams. In addition, our colleagues at Goddard, D. Howell, H. Burdick, R. Hoffman, J. Seek, and J. Scheifele, contributed significantly in the phases of the mission concerned with the magnetometer boom, instrumentation, and data analysis. Lastly, we recognize the contributions of the technical teams at Jet Propulsion Laboratory and the Boeing Company to the successful conduct of the overall mission; we especially acknowledge J. Bruns of Boeing in connection with this experiment.

29 May 1974

Electrons and Protons Accelerated in Mercury's Magnetic Field

Abstract. *Fluxes of protons with energies of* ~ 550 *kev and electrons with energies of* ~ 300 *kev which exceed approximately* 10^4 *and* 10^5 cm^{-2} sec^{-1}, *respectively, have been discovered in the magnetosphere of Mercury. Electron fluxes* $> 10^3$ cm^{-2} sec^{-1} *also are observed in the outbound pass of the Mariner 10 spacecraft through the magnetosheath. The intensity versus time profiles of the particle fluxes in the magnetosphere appear with sudden onsets of* $\sim 10^4$ cm^{-2} sec^{-1} *beginning at interplanetary background levels and persisting for times equivalent to their being distributed spatially over regions having a scale size comparable to the planetary radius. For a spectral form* $dJ/dE \propto E^{-\gamma}$, *where* J *is the differential particle intensity and* E *is the kinetic energy, the typical values of* γ *are* $\gamma_p = 5.5$ *for protons above 500 kev and* $\gamma_e \geqq 9$ *for electrons above 170 kev. Large coherent electron intensity oscillations (variations of factors of 10 to 100) have been discovered with characteristic periods of* ~ 6 *seconds and with higher frequency components. In some cases proton bursts are found in phase with these oscillations. On the basis of the experimental evidence and a knowledge of the general magnetic field intensities and directions along the trajectory of Mariner 10 provided by the magnetic field observations, it is shown that the radiation events observed in the magnetosphere and magnetosheath are transient and are not interpretable in terms of stable trapped particle populations. Furthermore, experimental evidence strongly supports the view that the particles are impulsively accelerated and that the acceleration source is not more distant from the point of observation along lines of force than* $\sim 8 \times 10^3$ *to* 16×10^3 *kilometers (3 to 6.5 units of Mercury's radius). Candidates for the regions most likely to be sources of particle acceleration are discussed, namely, the magnetotail and the magnetosheath. It is pointed out that the phenomena discovered at Mercury will place more stringent conditions on allowed models for electron and proton acceleration than have heretofore been possible in studies within the earth's magnetosphere.*

One of the outstanding problems of common interest for planetary electrodynamics and high energy astrophysics is the acceleration of electrons and protons arising from the solar wind interaction with the induced or intrinsic magnetic fields of the planets. A wide range of in situ measurements already made at four planets and at the moon serve as a basis for an investigation of the physical conditions necessary for particle acceleration. Only at the earth and Jupiter, which have intrinsic magnetic fields with extensive magnetospheres, has local acceleration been shown to exist for both trapped radiation and impulsive events of electrons and protons. For Venus and Mars, without intrinsic magnetic fields but with ionospheres which provide a conducting surface for the interaction with the solar wind, induced magnetic fields are generated and standoff bow shocks have been observed. No evidence has been found for particle acceleration above an energy of ~ 50 kev in either the bow shock or the plasma wake region of either Venus or Mars. The moon represents the extreme case of a solid body without appreciable intrinsic magnetic field, ionosphere, or any conducting surface to deflect the solar wind. It has neither a bow shock nor significant induced magnetic fields which could lead to charged particle acceleration. Therefore, in attempts to predict the conditions for particle acceleration at Mercury the evidence derived from these earlier studies suggested that unless Mercury had a significant intrinsic magnetic field (*1*, *2*), which was believed doubtful on the basis of its slow rotational period (*3*), the planet would most likely have a moonlike interaction with the solar wind (*1*, *4*, *5*). This prediction was supported by the fact that nonthermal radio emissions from Mercury had not been detected. Hence it appeared most probable that we would find no locally accelerated electron or proton fluxes in the 100-kev energy range associated with Mercury.

This is a preliminary report of our measurements from the Mariner 10 spacecraft, which show the presence at Mercury of large and impulsive fluxes of electrons with energies > 170 kev and protons with energies > 500 kev distributed over regions comparable in size to the planet itself. Our observations reveal physical conditions substantially different from those predicted for Mercury (*1*, *2*) based on the analogies mentioned above with other planets and the moon. The observed